Fermi National Accelerator Laboratory

FERMILAB-Conf-94/151-E

CDF

Evidence for Color Coherence in Jet Events

The CDF Collaboration

Fermi National Accelerator Laboratory
P.O. Box 500, Batavia, Illinois 60510

June 1994

Submitted to the *27th International Conference on High Energy Physics*, Glasgow, Scotland, July 20-27, 1994

Disclaimer

ICHEP94 Ref. 0406

Submitted to Pa 11

Pl 13

CDF Note 2614

26 May 1994

FERMILAB-CONF-94/151-E

Evidence for Color Coherence in Jet Events

The CDF Collaboration [1]

Abstract

Color coherence effects in $p\bar{p}$ collisions are observed and studied with CDF, the Collider Detector at the Fermilab Tevatron collider. We demonstrate these effects by measuring spatial correlations between soft and leading jets in multi jet events. Variables sensitive to interference are identified by comparing the data to the predictions of various shower Monte Carlos that are substantially different with respect to the implementation of coherence.

PACS numbers: 13.87.-a, 12.38.Qk, 13.85.-t

[1]Contributed by Paola Giannetti, Istituto Nazionale di Fisica Nucleare, Pisa; GIANNETTI@PISA.INFN.IT

Submitted 27th International Conference on High Energy Physics, University of Glasgow, Glasgow, Scotland, July 20-27, 1994

I. INTRODUCTION

Color coherence phenomena have been clearly observed in e^+e^- collisions [1, 2] and thoroughly examined from a theoretical point of view [3]. Owing to difficulties in detecting unambiguous effects in the data, however, we still lack significant experimental checks in $p\bar{p}$ collisions. Here, we report the first direct evidence for such effects observed in a hadron collider experiment, using 4.2 pb^{-1} of data collected by the Collider Detector at Fermilab (CDF) during the 1988-89 run of the Tevatron collider.

The most striking consequence of color coherence phenomena in QCD is given by the inhibition of soft radiation emission [4]. One way in which this interference manifests itself, is the so called *string effect* [1, 2, 3], whereby the amount of soft radiation emitted in the region between the two quark jets in a $e^+e^- \rightarrow$ 3-jet event is suppressed with respect to the region between the quark and the gluon jets. This effect is understood as the result of destructive interference between amplitudes with soft gluons emitted by color connected partons. Fig. 1 serves to clarify this point. The lines connecting the two quarks with the gluon represent the flow of the color charges involved in the process, and can be identified as antennas for the emission of additional color radiation. QCD predicts that these antennas behave approximately like standard dipoles, and therefore the radiation is concentrated mainly in the two regions towards which the antennas are pointing.

Similar graphs can be obtained for any QCD hard process, in particular for hadronic collisions where initial state colored partons are involved. Depending on the details of the hard scattering, different color flows are involved, and several color patterns can contribute to the same process. The multitude of possible color flows

participating in a hadronic process makes it very hard to identify a characteristic emission pattern. Until now, this has been one of the two major obstacles in obtaining compelling experimental evidence for these phenomena. The other obstacle that has prevented the identification of a clear signal is the difficulty of separating the contribution of soft particles produced by the underlying event: whilst these are expected to be distributed, on average, isotropically in azimuth (ϕ) and pseudorapidity ($\eta = -\log(tan\theta/2)$), event by event fluctuations in their distributions will bias any attempt to identify intrinsic asymmetries of the soft radiation produced in the hard scattering.

In this article, we show how it is possible to overcome both of these difficulties. We use the high energies available at the Tevatron to select events where the energy of the leading jets is so large that soft radiation is hard enough to form secondary jets. The spatial correlations between these secondary jets and the leading ones will give us variables similar to those used in the study of the string effect in e^+e^- collisions. A systematic comparison of the results with the predictions of some of the available theoretical calculations based on shower Monte Carlo generators will give evidence that what we are observing is indeed the result of color coherence. Preliminary results of this analysis have already been reported [5]. Preliminary results have also been presented recently by the D0 collaboration [6].

The outline of the paper is as follows: in Sec. II we cover in more detail the physics ideas underlying this measurement; we review the way different theoretical calculations incorporate these ideas and introduce the variables that will be used in the present analysis. In Sec. III we describe the triggers and the data selection criteria. Here we will also describe the generation of the Monte Carlo samples used for

the comparison of the data with the theoretical expectations. In Sec. IV we present and compare the data to the Monte Carlo results. In Sec. V, finally, we report the conclusions.

II. CONSTRUCTION OF VARIABLES SENSITIVE TO COHERENCE

As mentioned in the Introduction, color coherence leads to a suppression of soft gluon radiation in certain regions of phase space. Theoretical studies [4] show that these effects can be implemented in a shower Monte Carlo evolution by properly constraining the phase space allowed for the emission. In the case of final state showers (time-like evolution), this is achieved by requiring the emission angle in subsequent branchings to be decreasing and the radiation to be limited to lie within cones defined by color flow lines. This prescription is shown in Fig. 2, and is known as angular ordering.

Final state coherence is included in the shower Monte Carlos HERWIG [8] and PYTHIA [9], but is absent in ISAJET [10]. Monte Carlo programs including coherence via angular ordering in final state cascades have been extensively and successfully used to describe features of the experimental data in e^+e^-experiments [1, 2].

The phase space constraint in the case of radiation from an incoming initial state parton (space-like evolution) is slightly more complicated [11], but still amounts qualitatively to an angular ordering, with emission angles increasing as one moves from the initial hadron to the hard subprocess. A memory is retained of the shower initiator direction, even after many branchings. So far, HERWIG is the only program to fully include this kind of coherence.

In addition to constraining the independent evolutions of space-like and time-like

showers, color coherence gives a prescription for the emission of the first gluon from initial and final state partons [8, 12]. This prescription is required in order to provide the correct boundary conditions for the evolution of the initial and final states. We will consider as an example the case of $2 \to 2$ scattering. Each contributing process is decomposed into the various possible color flow configurations. In the approximation that neglects suppressed interference terms [7, 8, 12], all of the color configurations for the $2 \to 2$ process add incoherently to the total scattering probability. Then, each color configuration defines radiation cones in which partons can emit, following the angular ordering constraint defined for time-like showers. An explicit example is given in Fig. 3. In this particular example, the color lines flow from the initial to the final state partons, creating asymmetries in the structure of the observed soft radiation that are unique to collisions involving hadrons in both the initial and final states. These initial-final state color interference effects cannot be found in e^+e^- reactions, and have not been observed so far. PYTHIA includes these interference effects at the non-perturbative level via string fragmentation, but only HERWIG takes them into account within the perturbative evolution.

In this study, we intend to concentrate on observables which emphasize these initial-final state coherence effects and which allow us to disentangle them from the more standard final state coherence, already observed and tested in e^+e^- physics. Consider Fig. 4, which shows the spatial distribution of radiation for the hard $2 \to 2$ scattering displayed in Fig. 3. In this example, the emitting antenna is the line connecting partons 1 and 2. We define regions A and B, respectively, as the allowed emission cones for parton 1 and 2 as defined by the angular ordering prescription. The two cones overlap in region C, which is therefore a region of unsuppressed radiation.

In the region complementary to A and B the soft emission is forbidden.

Smaller scattering angles in the laboratory frame, θ_s, correspond to tighter phase space constraints. Our ignorance of the color topology prevents us from unequivocally determining the restriction cones for each observed event. Therefore, the aim is to identify variables that preserve some amount of the statistical correlations introduced by the restriction cones. Notice that, because of transverse momentum conservation, if the gluon forming the additional jet is emitted in region B, the jet recoiling against parton 2 will become the leading-E_T jet of the event. Parton 2 and the emitted gluon will, therefore, most often form the second- and third-E_T jets of the event. This suggests considering correlations between the directions of the second and third jet in the event.

We will measure the spatial distribution of the third jet around the second one using the distance in pseudorapidity, $\Delta\eta = \eta_3 - \eta_2$, and the distance in the azimuthal angle, $\Delta\phi = \phi_3 - \phi_2$. In order to better single out the region of maximum emission, we introduce the variable $\Delta H = sign(\eta_2) * \Delta\eta$. $\Delta H > 0$ corresponds to the region A in the example of Fig. 4.

Fig. 5 shows the density of the third-E_T jets in the $(|\Delta\phi|, \Delta H)$ space for the data sample to be defined in the next section. The azimuthal distance $|\Delta\phi|$, shown on the horizontal axis, spans the range [0, π], whereas, ΔH, shown on the vertical axis, is constrained by the calorimeter acceptance to be in the range $|\Delta H| < 4$. For each event, the second jet is located at the origin, while the first jet is expected to be more or less back to back in ϕ, that is near the edge $|\Delta\phi| = \pi$. The position of the third jet axis is represented by a point in the plane.

Since the jets have been reconstructed using a fixed-cone clustering algorithm

[13, 14] with cone radius $R_{cone} = 0.7$, the circular region of radius R_{cone} in the $(|\Delta\phi|, \Delta H)$ space around the second jet axis is forbidden to other jets. Therefore, a set of "polar" variables turns out to be useful. We define $R = \sqrt{(\Delta\eta^2 + \Delta\phi^2)}$ and $\alpha = atan(\Delta H/|\Delta\phi|)$ as our variables of choice. The variable R is the distance between the third and second jet in the (η, ϕ) space. The variable α is the polar angle in the $(|\Delta\phi|, \Delta H)$ space.

In Fig. 6 the regions A, B, and C of Fig. 4 are mapped on the (α, R) space. The black region on top is forbidden by the limits $|\Delta\phi| < \pi$, while the straight line at $R = R_{cone} = 0.7$ shows the boundary around the second jet axis, generated by the clustering algorithm. Limits imposed by the CDF calorimeter acceptance are not shown. The figure illustrates the boundaries imposed by the angular ordering restriction for the case of $\theta_s = 85°$.

We then expect the distributions of variables such as α and R to be sensitive to the phase space constraints imposed by the color interference.

In conclusion, we plan to use the α and R variables to exhibit color coherence. We will also study the absolute pseudorapidity of the third jet, η_3. Color coherence is expected to broaden the η_3 distribution, increasing the probability of having third jets at large pseudorapidities. This is because the coherent emission "remembers" the first prong of the radiating antenna, that is, the beam line.

III. THE DATA AND THE MONTE CARLO SAMPLES

A. The Data Sample

The CDF detector has been described in detail elsewhere [15].

The data were collected using a single-jet online trigger, which required at least

one cluster of transverse energy $E_t = Esin\theta$ greater than a threshold of 60 GeV.

The uncorrected energy of a jet is defined by the clustering algorithm [14] as the scalar sum of the measured energies in the electromagnetic and hadronic compartments within a cone around the cluster centroid. The momentum of the cluster is calculated by assuming that the energy in each calorimeter tower belonging to the cluster is deposited by a massless particle hitting the center of the tower.

The measured energy and momentum of each jet are corrected, on average, for detector effects: degradation of the measurement due to calorimeter non-linearity, uninstrumented regions of the detector and bending of charged particle tracks in the CDF 1.4 T solenoid magnetic field in the central region. The absolute energy response is derived [17] from Monte Carlo jets generated in the central region and processed through a full detector simulation. The average energy degradation is 17% (12%) at 35 (300) GeV. The Monte Carlo program is tuned to reproduce (a) the charged particle fragmentation of jets observed in the data and (b) the calorimeter response to single charged pions and electrons (measured in a test beam) and to single isolated charged particles in the data from $p\overline{p}$ collisions. The true jet energy (E) and momentum (p) are defined as the total energy and momentum of all the particles (leptons, photons, and hadrons) emerging from the primary vertex within a cone of fixed radius R_{cone} around the cluster centroid. No attempt is made to reconstruct the energy of the parton from which the jet originates, e.g. no corrections are applied to account for energy lost out of the clustering cone or to account for the underlying event. Our energy scale corrections are intended to produce an unbiased estimate of the true jet 4-momentum (E, p), defined above. To measure the relative response of the detectors at large pseudorapidity, jet p_T balancing is used. The method is fully

described in references [17], [18].

The cosmic ray background is rejected with criteria described in reference [19]. Events with a significant missing transverse energy are rejected if one of the two leading jets has an electromagnetic fraction smaller than 0.05 or greater than 0.95. The missing transverse energy significance is calculated as $(MET)^2 = [(\Sigma E_T sin\phi)^2 + (\Sigma E_T cos\phi)^2]/(\Sigma E_T)$, with E_T measured in GeV, and is required to satisfy $MET > 6$. The E_T-sums include only the energy that has been clustered into jets.

The criteria for the event selection are listed below.

1. The event vertex along the beam line is required to be within 60 cm of the center of the detector.

2. The two leading jet axes (i.e., those with the highest transverse energies) are required to be in the pseudorapidity ranges $|\eta_1|, |\eta_2| < 0.7$. Coherence effects are expected to increase for smaller scattering angles. However, this selection ensures that the two leading jet cores are well contained in the central calorimeter, that has the best energy resolution. Fluctuations in the energy measurements smear the coherence effects [20].

3. $||\phi_1 - \phi_2| - \pi| < 20°$; the two leading jets are required to be back to back within 20° in the transverse plane. This is a loose cut to select events with soft radiation, which are well described in the approximation of the shower Monte Carlos.

4. The measured transverse energy of the first jet in the event, E_{T1}, is required to be large enough such that it is free of biases introduced by the trigger threshold. The corrected E_{T1} threshold above which our data selection is fully efficient is

110 GeV. This 100% efficiency point is measured through the use of lower trigger threshold data.

5. The presence of a third jet is required. In order to avoid the possible background due to underlying event fluctuations, the third jet corrected transverse energy, E_{T3}, is required to be greater than 10 GeV.

6. This last selection requirement is applied only for the study of the α variable: a rectangular region of uniform acceptance in the scatter plot α versus R (Fig. 6) is chosen by requiring that $1.1 < R < \pi$. The former condition removes the sharp rise due to the clustering algorithm, whilst the latter condition discards the upper region of the α dependent acceptance.

B. The Simulated Samples

We use different shower Monte Carlos to generate jet events that are subsequently processed by the CDF detector simulator.

The Monte Carlo HERWIG (version 3.2) imposes proper phase space constraints on soft emissions from any kind of color antenna, including those spanned between the initial and final states (initial-final state antenna).

The Monte Carlo ISAJET (version 6.25) does not implement angular ordering in the initial or the final state radiation.

The Monte Carlo PYTHIA (version 5.6) imposes proper phase space constraints only on soft emissions of time-like shower evolutions. In particular, this does not include initial-final state antennas. PYTHIA was written when theoretical results pertaining to coherence were available only for the time-like shower evolution, and does not implement the more complicated angular ordering of the space-like shower

evolution. This approximation is appropriate for describing e^+e^- results, or for studying W/Z events in $p\overline{p}$ collisions, where there is no interference between initial and final state.

Since we intend to concentrate on initial-final state color interference effects, we also use a new version of PYTHIA, expressly provided by the author T. Sjöstrand, which implements the phase space constraints for the initial-final state antennas [21] as well. This version will be called PYTHIA+ [2].

PYTHIA has a feature that allows one to switch on and off the simulation of color coherence, without altering any other feature of the event generation. We have generated a sample of PYTHIA events with no simulation of color coherence (PYTHIA-off).

We have generated all the samples with transverse momenta p_T of the final state partons greater than 75 GeV. Since our analysis involves only central leading jets, we have constrained the final state partons to lie in the rapidity interval $|y| < 1.5$, hence achieving high statistics with the least CPU-time. Control samples, with a smaller p_T threshold and a greater rapidity interval, have been generated to check for the absence of biases introduced by the above generation cuts in the selected samples.

In addition to the standard CDF simulation, we have also processed the generated events through a fast simulation of an ideal calorimeter where the particle's energy is exactly measured. The tower segmentation of the ideal calorimeter is the same of the real one, but with no dead regions. The output of the fast simulation is then processed by the standard clustering algorithm, that in this case defines precisely "measured" jets. The primary vertex is always at the center of the detector and no

[2]These modifications are now implemented in the latest version of PYTHIA, 5.7

magnetic field is simulated.

We have generated 280000 events for each sample, corresponding to the integrated luminosities listed in Table 1. This table also lists the number of events in the samples after the different selection cuts.

We make use of the Monte Carlo samples to understand how the color coherence reveals itself in the spatial distribution of the third-E_T jet. Fig. 7 shows a comparison between the samples of PYTHIA+ and PYTHIA-off. The distributions of the variables η_3, R, and α of one sample are superimposed, on an absolute scale, to those of the other sample. The distributions are normalized to the same integrated luminosity. The ideal calorimeter simulation is used in order to obtain a comparison independent of the CDF detector details. Since the only difference between PYTHIA+ and PYTHIA-off is in the simulation of the color coherence, Fig 7 illustrates that the interference depletes selected regions of the distributions. The depletion is, of course, a direct consequence of the radiation suppression outside the restriction cones. The total probability for generating a third jet becomes smaller, as can also be seen from Table 1.

In order to bypass the problem of large cross section uncertainties in the comparison between data and Monte Carlos, in what follows all the distributions represent probabilities normalized to unit area; i.e., only the shapes of the distributions are compared. Fig. 8 compares the distribution shapes of the same variables η_3, R, and α for several Monte Carlo samples. PYTHIA and PYTHIA-off do not show a significant difference. This means that the degree of color coherence implemented in the PYTHIA sample is not enough to exhibit an effect on the examined distributions. On the contrary, HERWIG and PYTHIA+ agree each other but show a substantial

difference from PYTHIA-off. This suggests the possibility of recognizing color coherence effects in the data by comparing the measured distributions of η_3, R, and α to those predicted by different Monte Carlos.

IV. COLOR COHERENCE IN THE DATA

In order to exhibit the color coherence effects, we compare the data to the predictions of the different shower Monte Carlos. Unless otherwise specified, all of the distributions presented in this paper represent probabilities and are normalized to unit area. The distributions are uncorrected for detector effects, such as finite resolution smearing and uninstrumented regions; these effects are included in the detector simulation. The error bars shown on the data points are statistical errors only. The main systematics are discussed in [20], and are shown to be small.

For each Monte Carlo sample we first check that the distributions for the pseudorapidities and transverse energies of the two leading jets are in good agreement with the data. This gives us confidence that the main hard scattering features are reproduced by all the physics generators. In order to illustrate the typical level of agreement between data and all of the Monte Carlos, we show in Figs. 9 and 10, the comparison between the transverse energy distributions for the real and the simulated data.

In direct contrast, the distributions of variables sensitive to interference exhibit differences between the different Monte Carlos. Fig. 11 shows the third jet pseudorapidity (η_3) distributions for HERWIG (a), ISAJET (b), PYTHIA (c), and PYTHIA+ (d), superimposed on the data. The distributions of HERWIG and PYTHIA+ agree better with the data than those of ISAJET and PYTHIA, which are narrower and

have a clear excess of events at small η.

Figs. 12 and 13 show similar comparisons for the variables R and α defined in Sec. II. Again, HERWIG (a) and PYTHIA+ (d) reproduce the data better than ISAJET (b) and PYTHIA (c). The coherence effect in Fig. 13 is observable as a change of the slope sign for $\alpha \to \pi/2$. This change is present in the data, HERWIG and PYTHIA+ distributions. The ISAJET and PYTHIA distributions, instead, are monotonically decreasing from $\alpha = -\pi/2$ to $\alpha = \pi/2$ and show a clear excess of events at small $|\alpha|$ values. What we observe is consistent with the expectations of Sec. II where the region near $\alpha = \pi/2$ is predicted to be the only one not depleted by destructive interference (see also Fig. 7c in Sec. III B). A representative comparison of the data and theory is obtained using the quantity (Monte Carlo)/DATA (Fig. 14). The α distribution shown in Fig. 13 for each Monte Carlo is divided bin by bin by the data distribution, also shown in Fig. 13. Again the Monte Carlos that do not take into account initial-final state interference (Fig. 14b,c) show a clear excess of events in the regions expected to be more depleted by color coherence. However, it should be noted that residual differences remain with the data, even in the case of HERWIG and PYTHIA+. For brevity, we will use the term "*interference patterns*" to refer to the shapes of the data distributions in Figs. 11, 12, and 13.

Since color coherence is approximated to different degrees in the four shower Monte Carlos considered, we can draw the following conclusions:

1. The variables R, η_3 and α discriminate between the Monte Carlos (see Figs. 11, 12, and 13).

2. The color coherence is responsible for the differences between the predictions. In fact, the agreement with the data improves as higher degrees of color coherence

are implemented. Moreover, these variations are in accord with the description of Sec. II. The η_3 distribution and, accordingly, the R distribution become wider. The α distribution shows the effect of the α-dependent suppression.

3. The *interference patterns* exhibit the color coherence in the data. The effect survives the non-perturbative phase of the hadronization as well as the smearing due to the underlying event.

V. CONCLUSIONS

We have presented in this paper direct evidence for color coherence phenomena in $p\bar{p}$ collisions. The result has been obtained by studying kinematical correlations between the second- and the third- most energetic jets in multijet events. We have compared our data with several shower Monte Carlo calculations that implement, with differing levels of accuracy, the quantum coherence in the gluon radiation process. The comparison of the shape of third jet distributions has allowed us to single out the interference between initial and final state gluon emission from color connected partons as the origin of the observed correlations. We have verified that HERWIG and a modified version of the PYTHIA Monte Carlo (now implemented in version 5.7) reproduce the data better than ISAJET and PYTHIA version 5.6. This confirms complementary findings from e^+e^-physics supporting the theoretical result that color coherence phenomena can be included in a shower Monte Carlo despite their quantum nature. It is expected that future quantitative studies, extending this analysis for example to different jet energy ranges or to different event samples, will provide additional tests of QCD color coherence and will result in further improvements in the theoretical models. Investigations should focus on the residual disagreements

remaining between the data and the predictions of the Monte Carlos implementing color coherence.

Given the relevance of the first emission in determining the third jet direction [20] we expect the parton level calculations [22] based on next-to-leading order QCD matrix elements [23] to be able to describe our measurements. As soon as the relevant calculations are available, it will be interesting to compare the distributions studied in this work with NLO predictions.

ACKNOWLEDGMENTS

We are deeply thankful to T. Sjöstrand for his constant and active interest in this work. His contribution was fundamental for our complete understanding and interpretation of the results. We thank the Fermilab Accelerator Division, the Computer Division, and the CDF technical staff for their dedicated effort that made this experiment possible. This work was supported by the Department of Energy, the National Science Foundation, the Natural Sciences and Engineering Research Council of Canada, the Italian Istituto Nazionale di Fisica Nucleare, the Ministry of Science, Culture and Education of Japan, and the A.P. Sloan Foundation.

References

[1] JADE Collaboration, W. Bartel et al., Phys. Lett. B **101**, 129 (1981); Z. Phys. C **21**, 37 (1983);

TPC/2γ Collaboration, H. Aihara et al., Phys. Rev Lett. **54**, 270 (1985); Z. Phys. C **28**, 31 (1985); Phys. Rev Lett. **57**, 945 (1986);

TASSO Collaboration, M. Althoff et al., Z. Phys. C **29**, 29 (1985);

MARK2 Collaboration, P.D. Sheldon et al., Phys. Rev Lett. **57**, 1398 (1986).

[2] OPAL Collaboration, M.Z. Akrawy et al., Phys. Lett. B **247**, 617 (1990);

OPAL Collaboration, M.Z. Akrawy et al., Phys. Lett. B **261**, 334 (1991);

OPAL Collaboration, P.D. Acton et al., Phys. Lett. B **287**, 401 (1992);

OPAL Collaboration, P.D. Acton et al., Z. Phys. C **58**, 207 (1993).

[3] For reviews, and ref.'s to the original literature see: Yu.L. Dokshitzer, V.A. Khoze and S.I. Troyan, in *Perturbative QCD*, ed. A.H. Mueller, Singapore: World Scientific (1989), 241;

Yu.I. Dokshitzer, V.A. Khoze, S.I. Troyan and A.H. Mueller, *Rev. Mod. Phys.* **60** (1988), 373.

[4] For a review, see: A. Bassetto, M. Ciafaloni and G. Marchesini, *Phys. Rep.* **100** (1983), 201.

[5] M. Dell'Orso, CDF Collaboration, Proceedings of the 8th Topical Workshop on Proton-Antiproton Collider Physics, 1-5 Sept. 1989, Castiglione della Pescaia (Italy), eds. G. Bellettini and A. Scribano, World Scientific Publ., 177;

R. M. Harris, CDF Collaboration, Proceedings XXVIIth Rencontres de Moriond, 22-28 March 1992, Les Arcs, Savoie (France) eds. J. Tran Thanh Van, Editions

Frontieres, 3;

E. Meschi, CDF Collaboration, Proceedings of the DPF Meet. Am. Phys. Soc., 10-14 Nov 1992, Batavia (Illinois), eds. C.H. Albright et al., World Scientific Publ., 1117.

[6] F. Borcherding, D0 Collaboration, Fermilab Report No. FERMILAB-Conf-93/388-E, 1993 (to be published in the Proceedings of the 9th Topical Workshop on Proton-Antiproton Collider Physics, 18-22 Oct. 1993, Tsukuba, Japan).

[7] H.-U. Bengtsson, *Comp. Phys. Comm.* **31** (1984), 323.

[8] G. Marchesini and B. Webber, Nucl. Phys. B **310**, 461 (1988).

[9] H.-U Bengtsson and T. Sjöstrand, *Comp. Phys. Comm.* **46** (1987), 43;
T. Sjöstrand and M. Bengtsson, *Comp. Phys. Comm.* **43** (1987), 367;
T. Sjöstrand, CERN-TH 6488 (1992).

[10] F. E. Paige and S. D. Protopopescu, BNL Report No. 38034 (1986).

[11] M. Ciafaloni, Nucl. Phys. B **296**, 249 (1987); S. Catani, F. Fiorani, G. Marchesini, Phys. Lett. **234**, 339 (1990);

[12] R.K. Ellis, G. Marchesini and B. Webber, *Nucl. Phys.* **B286** (1987), 643.

[13] J. Huth *et al.*, Proceed. of the Summer Study on High Energy Physics (1990), Snowmass, Colorado, 134.

[14] F. Abe *et al.*, Phys. Rev. D **45**, 1448 (1992).

[15] F. Abe *et al.* Nucl. Instr. Meth. A **271**, 387 (1988).

[16] F. Abe *et al.*, Phys. Rev. Lett. **65**, 2243 (1990).

[17] F. Abe *et al.*, Phys. Rev. D **45**, 1448 (1992).

[18] F. Abe *et al.*, Phys. Rev. Lett. **69**, 2896 (1992).

[19] F. Abe *et al.*, Phys. Rev. Lett. **62**, 613 (1989).

[20] F. Abe *et al.*, Fermilab Report No. FERMILAB-Pub-94/072-E, 1994 (to be published on Phys. Rev. D)

[21] T. Sjöstrand, private communication.

[22] S.Ellis, Z.Kunszt and D. Soper, *Phys. Rev. Lett.* **64** (1990), 2121;
F.Aversa, P.Chiappetta, M. Greco and J.P. Guillet, *Z. Phys.* **C46** (1990), 253.

[23] R.K. Ellis and J.C. Sexton, *Nucl. Phys.* **B269** (1986), 445. A.E. Chudakov, Izv, Akad, Nauk, SSSR Ser. Fiz. **19**, 650 (1955).

	Data	HERWIG	ISAJET	PYTHIA-off	PYTHIA+	PYTHIA
Luminosity (pb^{-1})	4.2	5.5	5.9	5.8	5.8	5.8
After cuts 1,2,3,4	13983	15706	16145	15143	14540	16181
After cut 5	10649	11004	12261	10565	9085	11988
After cut 6	8201	8474	9444	8382	6940	9411

Table 1: The number of events in the data and the simulated samples. Each simulated sample originally contained 280000 events. See text for definition of the cuts.

Figure Captions.

Fig. 1: Sketch of a $e^+e^- \to 3-jet$ event. a) Partons exiting from the primary vertex. Soft radiation, represented by shadowing, is suppressed in the region between the two quarks relative to the other regions. b) Color flow for the same event. The color lines can be identified as directional antennas.

Fig. 2: Angular ordering. a) Feynman diagram of a final state shower. b) Color flow in the shower. c) Partons exiting from the primary vertex. The emitted radiation is constrained around the emitting parton, within a cone defined by the color-connected partner. A similar cone (not shown) confines radiation emitted by the partner.

Fig. 3: Phase space constraints for the first gluon emission in a $q\overline{q}$ annihilation. a) Feynman diagram of the hard scattering. b) Color lines flow from the initial to the final state, q and q' are color partners. c) Restriction cones for q and q'. Similar cones can be drawn for $\overline{q}$ and $\overline{q}'$.

Fig. 4: Spatial distribution of radiation for the $2 \to 2$ scattering of Fig. 3. a) Radiation from the emitting antenna is maximum in the overlap region C. Soft emissions from the antenna are forbidden outside the restriction cones A and B. b) Cross section of picture a).

Fig. 5: The observed spatial distribution of the third jet around the second jet. Each point represents the position of a third-E_T jet. The second jet axis corresponds to the origin. The circular region around the second jet is forbidden to other jets by the clustering algorithm. The limit $|\Delta H| < 4$ is due to the calorimeter acceptance.

Fig. 6: The restriction cones of Fig. 4 as seen in the (α, R) space. The upper curved boundary corresponds to the limit $|\Delta\phi| < \pi$. The clustering algorithm prevents the jet axes from falling in the rectangular region $R < 0.7$. The boundaries between regions A, B, and C correspond to the case $\theta_s = 85°$.

Fig. 7: PYTHIA-off compared to PYTHIA+ on an absolute scale: (a) η_3 distribution; (b) R distribution; (c) α distribution.

Fig. 8: Comparisons between different Monte Carlo samples for the variables η_3 (1), R (2), and α (3): (a) PYTHIA-off compared to PYTHIA; (b) PYTHIA-off compared to HERWIG; (c) PYTHIA+ compared to HERWIG.

Fig. 9: Observed E_{T1} distribution compared to the predictions of: (a) HERWIG; (b) ISAJET; (c) PYTHIA; (d) PYTHIA+.

Fig. 10: Observed E_{T2} distribution compared to the predictions of: (a) HERWIG; (b) ISAJET; (c) PYTHIA; (d) PYTHIA+.

Fig. 11: Observed η_3 distribution compared to the predictions of: (a) HERWIG; (b) ISAJET; (c) PYTHIA; (d) PYTHIA+.

Fig. 12: Observed R distribution compared to the predictions of: (a) HERWIG; (b) ISAJET; (c) PYTHIA; (d) PYTHIA+.

Fig. 13: Observed α distribution compared to the predictions of: (a) HERWIG; (b) ISAJET; (c) PYTHIA; (d) PYTHIA+.

Fig. 14: Bin by bin ratio (Monte Carlo/DATA) of the (a) HERWIG, (b) ISAJET, (c) PYTHIA, (d) PYTHIA+ α distributions of Fig.13 over the data α distribution also shown in the same figure.

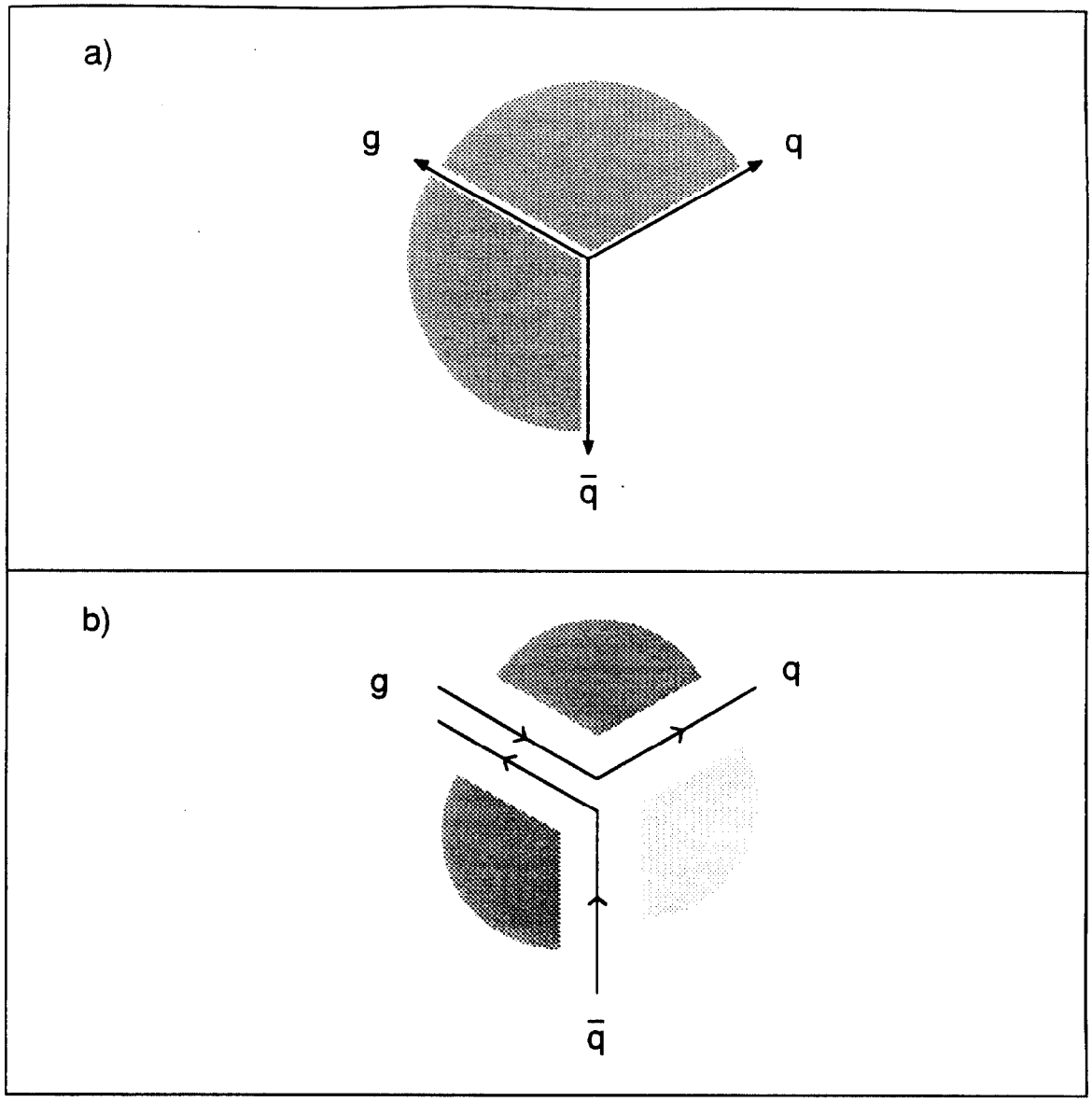

Figure 1:

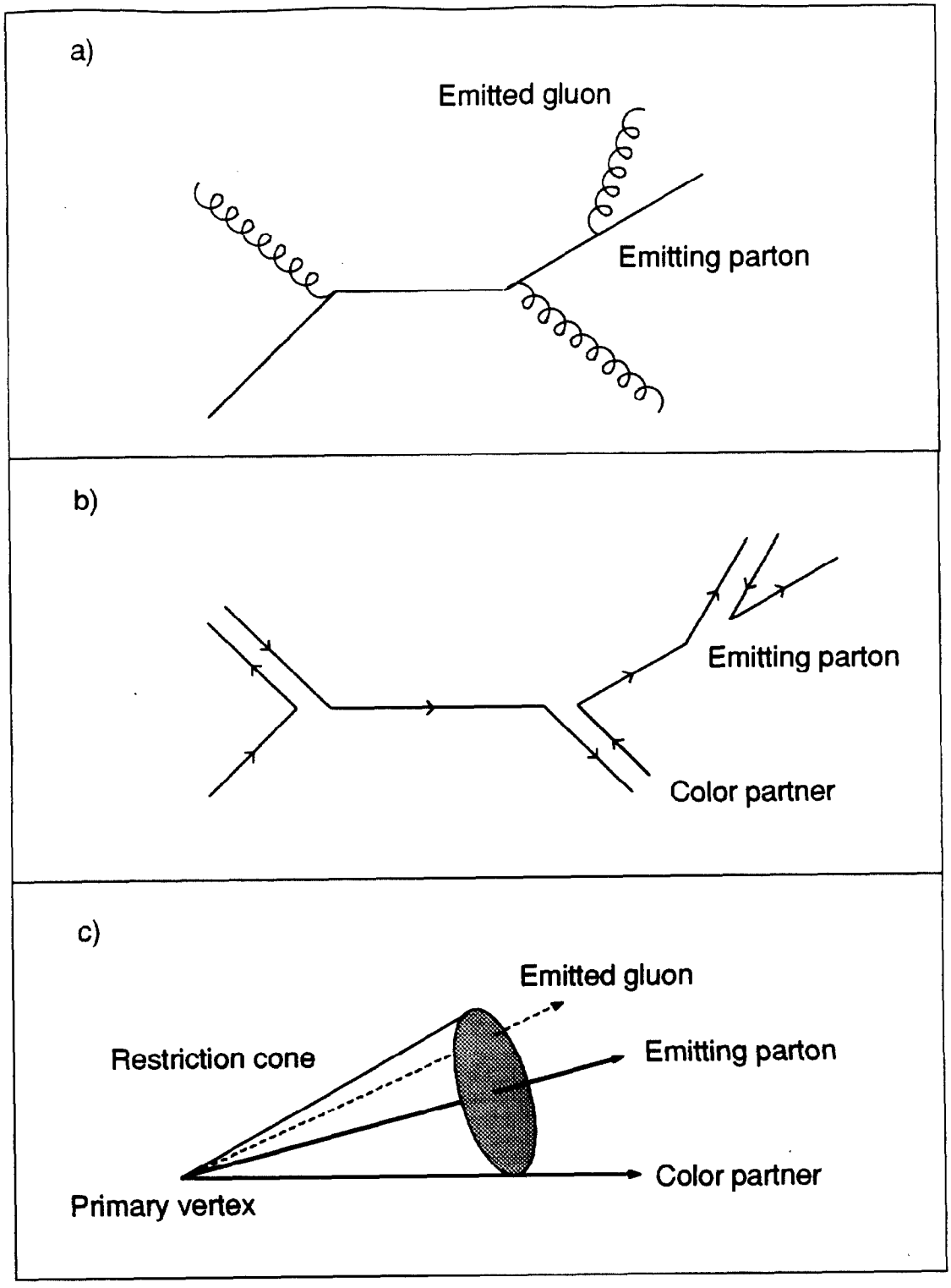
a)
Emitted gluon
Emitting parton
b)
Emitting parton
Color partner
c)
Emitted gluon
Restriction cone
Emitting parton
Color partner
Primary vertex

Figure 2:

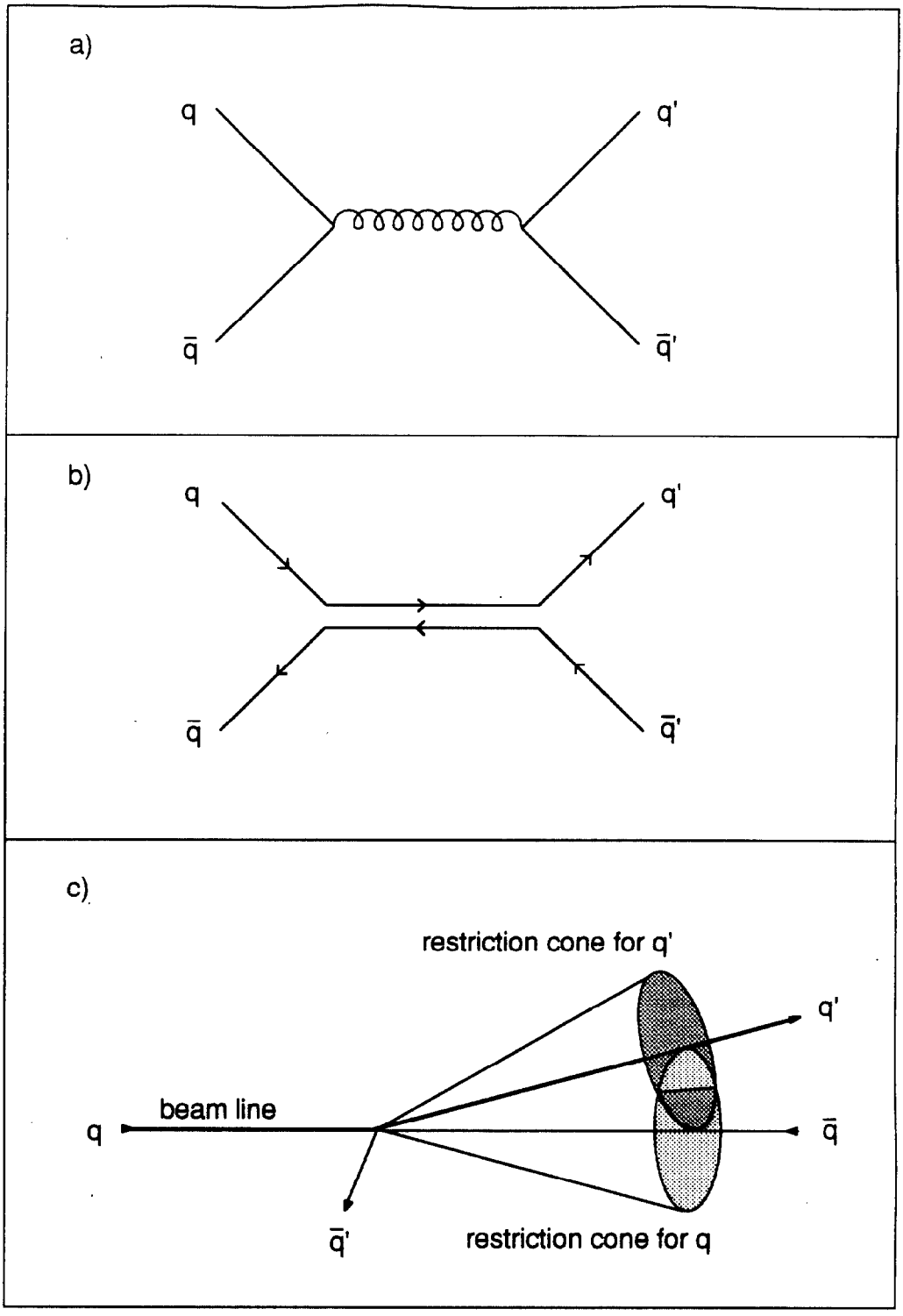
a)
q
q'
$\bar{q}$
$\bar{q}'$
b)
q
q'
$\bar{q}$
$\bar{q}'$
c)
restriction cone for q'
q'
beam line
q
$\bar{q}$
$\bar{q}'$
restriction cone for q

Figure 3:

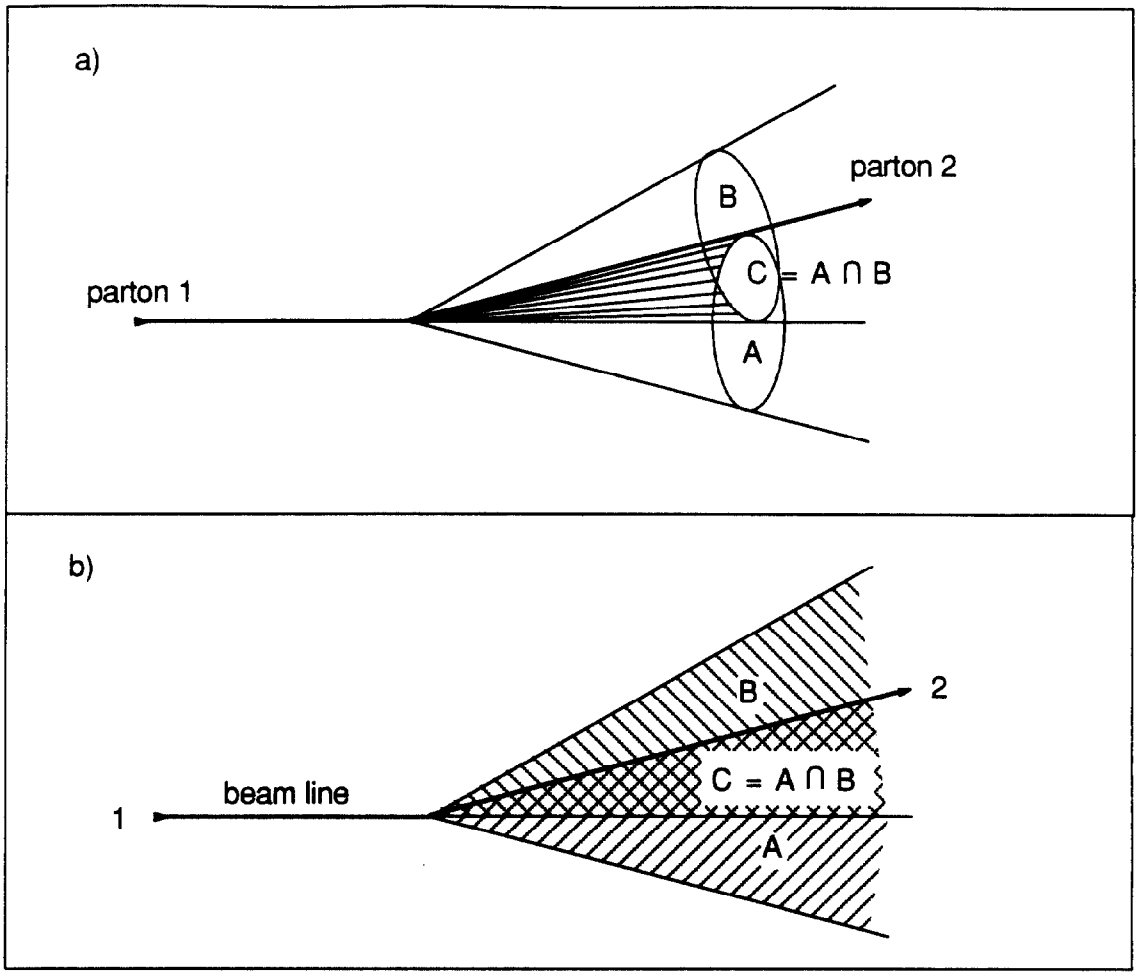

Figure 4:

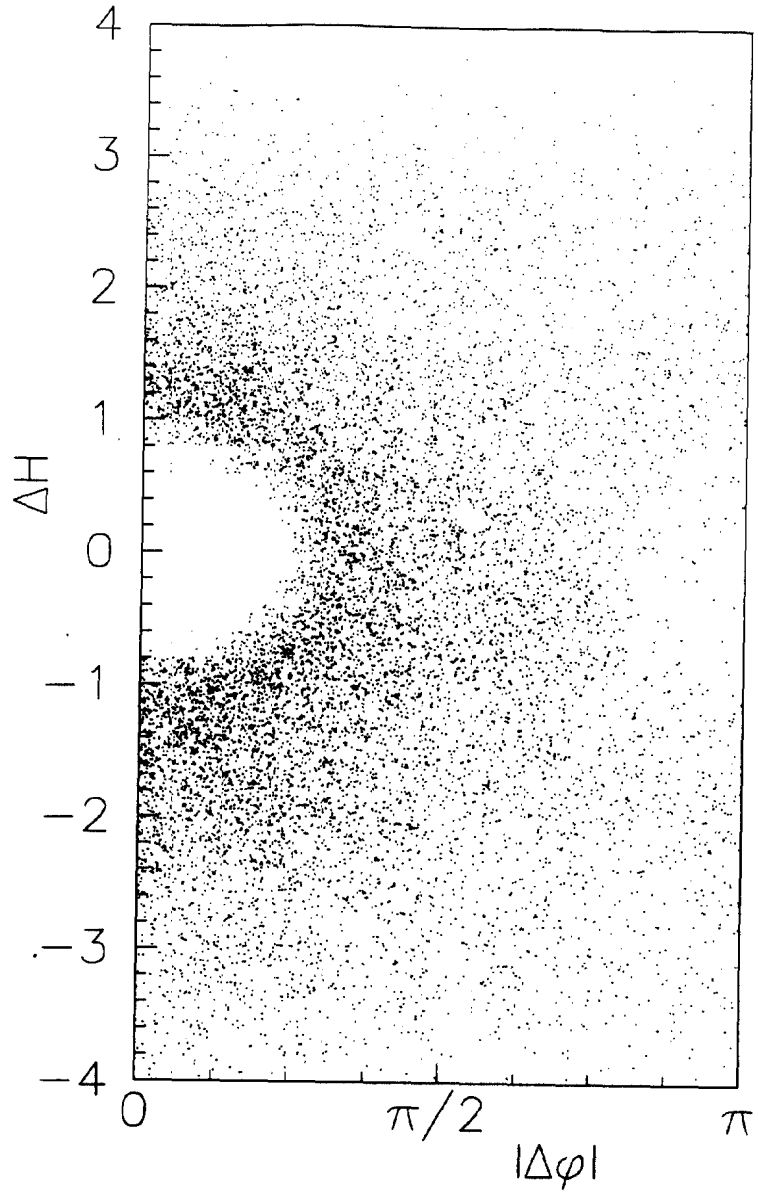

Figure 5:

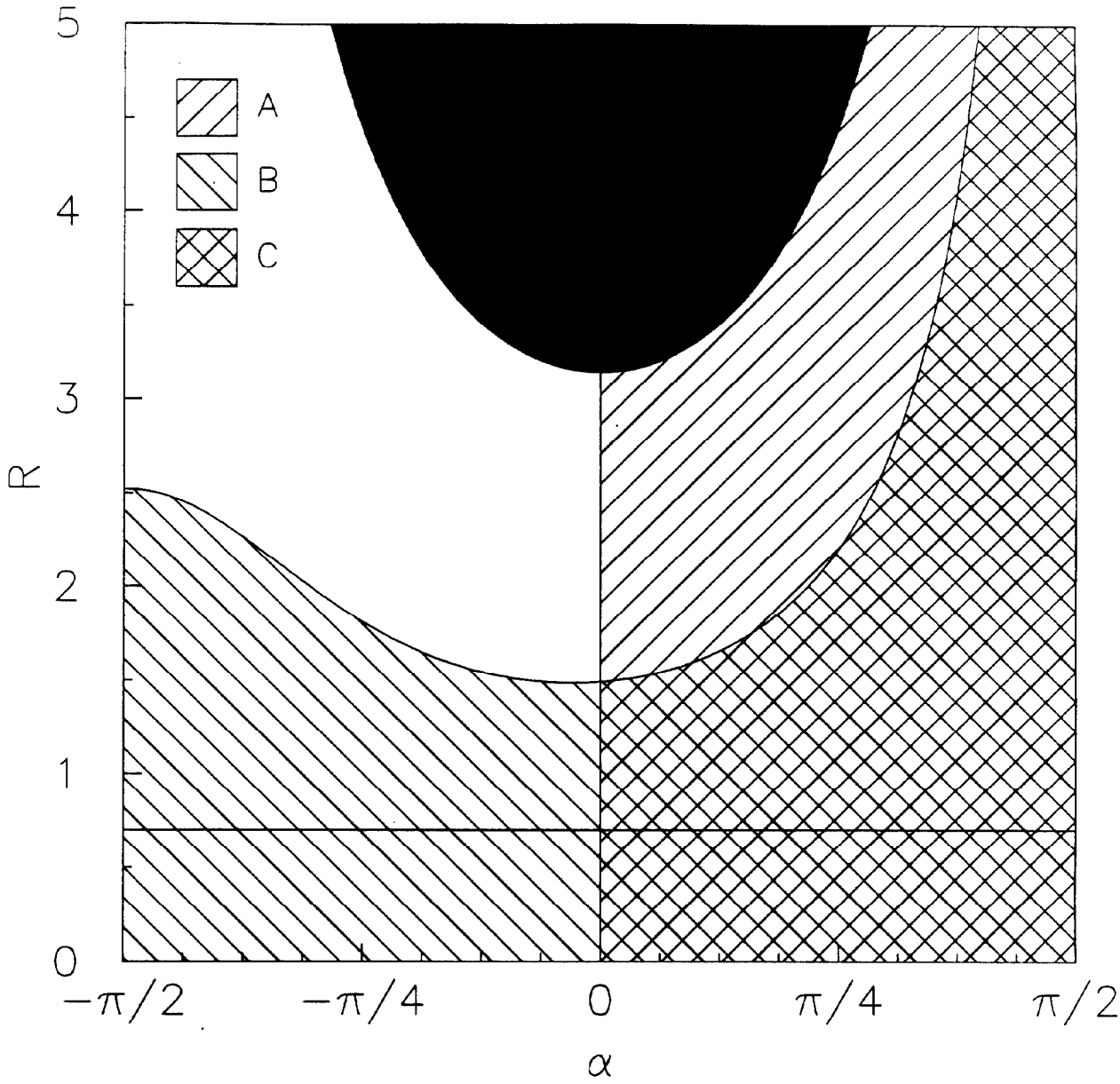

Figure 6:

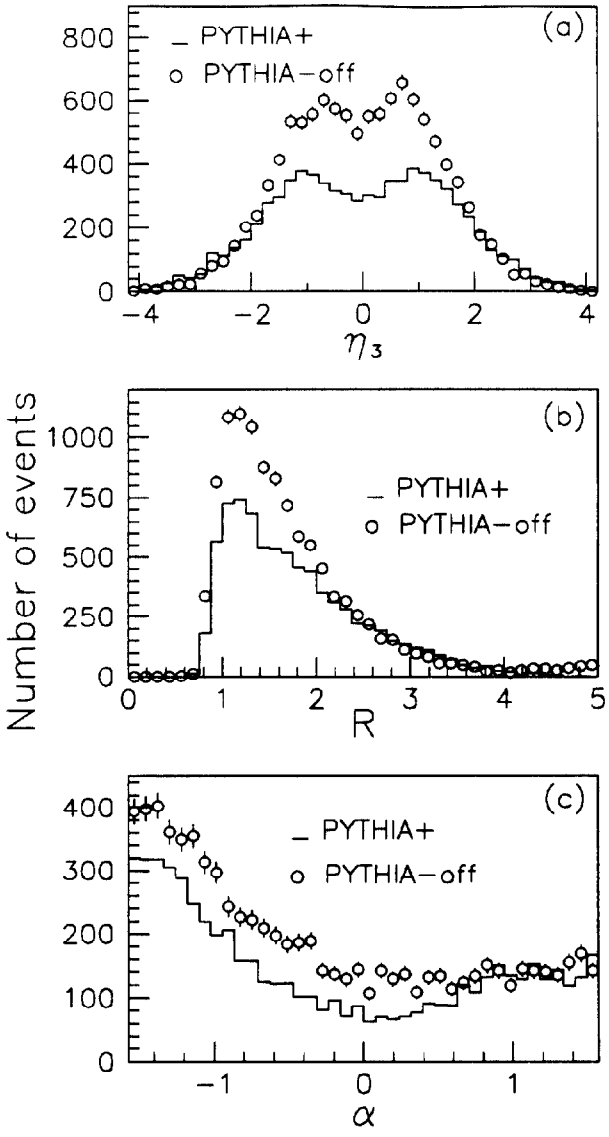
(a)
PYTHIA+
PYTHIA−off
800
600
400
200
0
−4
−2
0
2
4
η_3
(b)
PYTHIA+
PYTHIA−off
Number of events
1000
750
500
250
0
0
1
2
3
4
5
R
(c)
PYTHIA+
PYTHIA−off
400
300
200
100
0
−1
0
1
α

Figure 7:

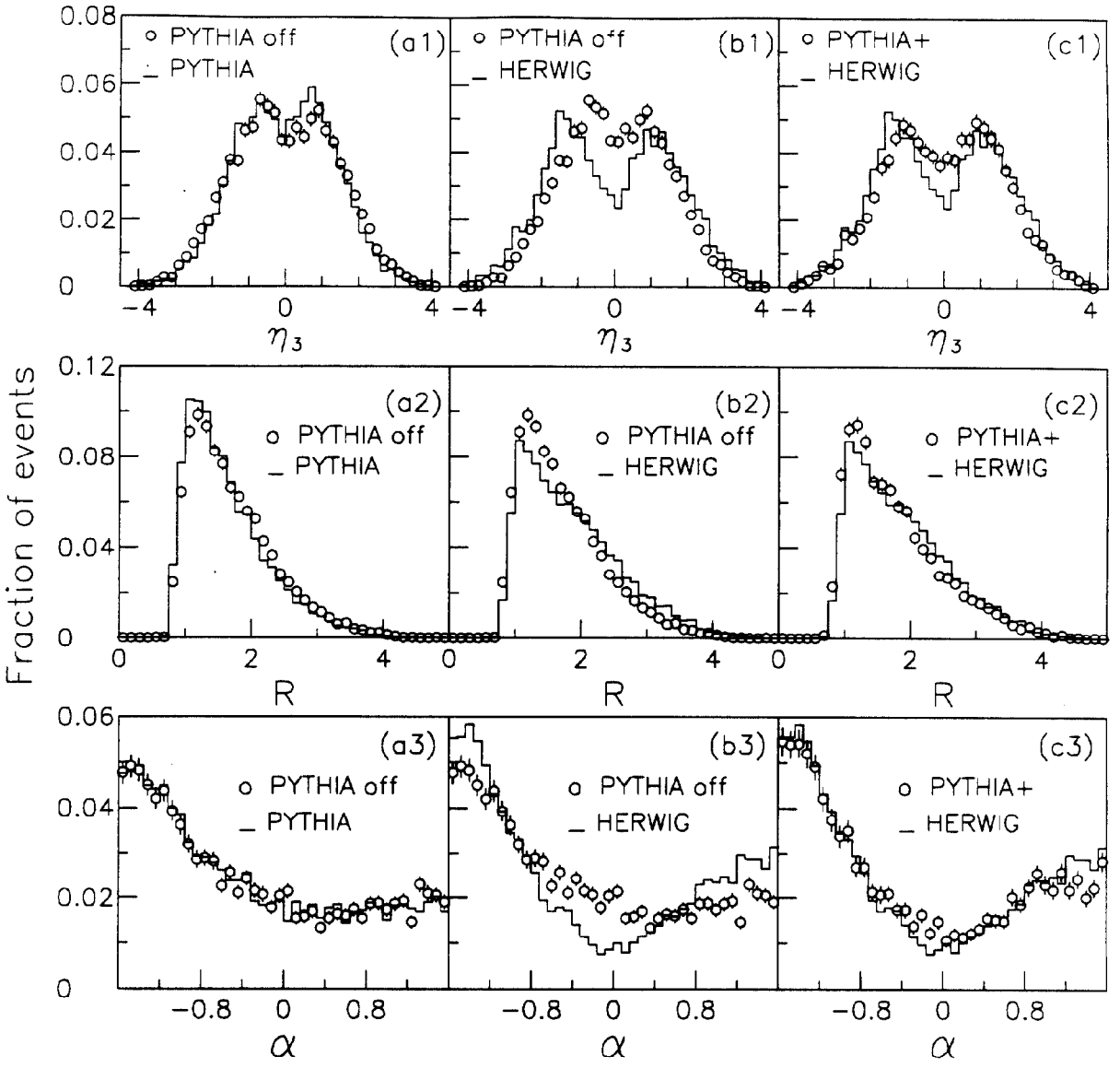
Fraction of events
(a1)
(b1)
(c1)
(a2)
(b2)
(c2)
(a3)
(b3)
(c3)
PYTHIA off
PYTHIA
HERWIG
PYTHIA+
η_3
R
α

Figure 8:

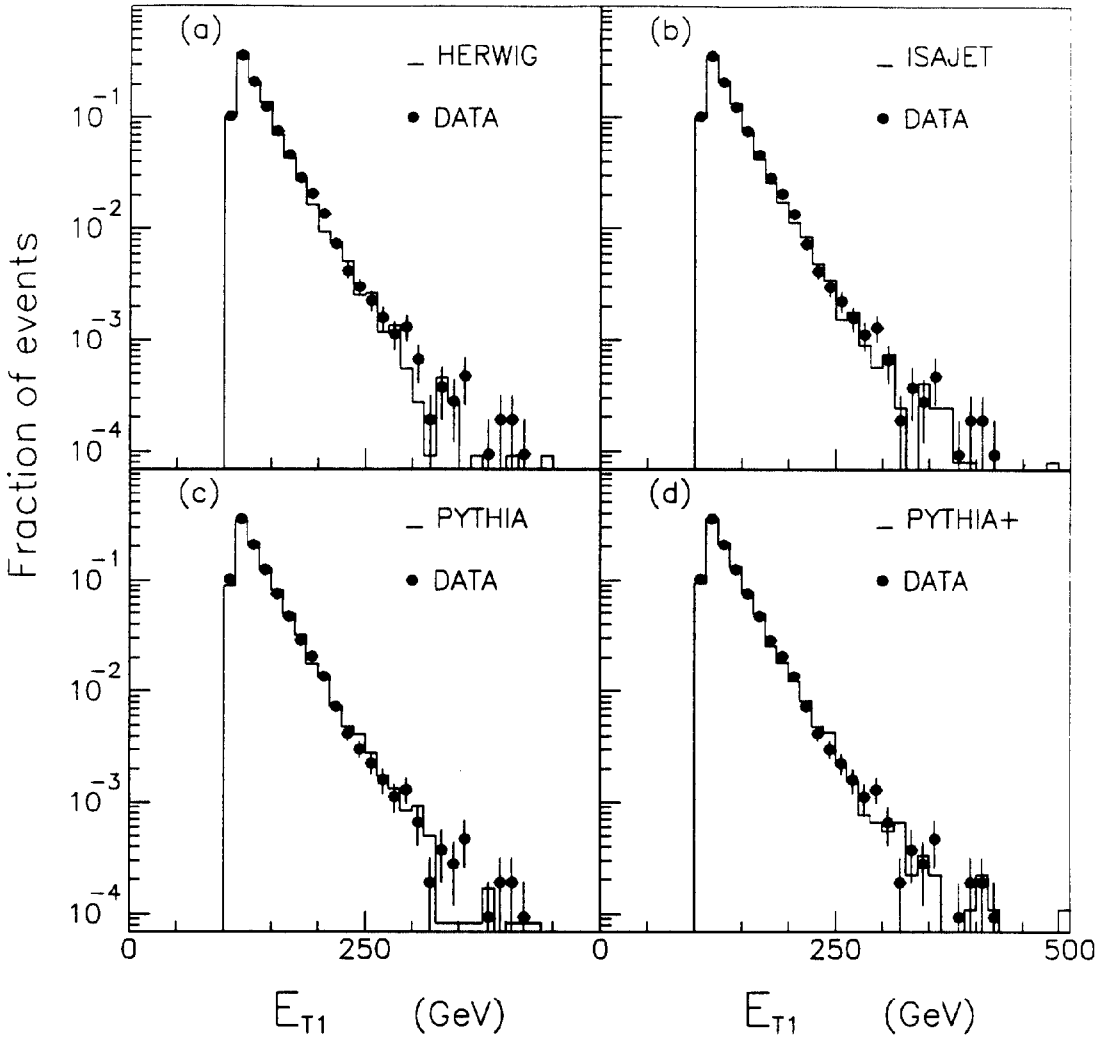
(a)
HERWIG
DATA
(b)
ISAJET
DATA
(c)
PYTHIA
DATA
(d)
PYTHIA+
DATA
Fraction of events
10^{-1}
10^{-2}
10^{-3}
10^{-4}
0
250
500
E_{T1} (GeV)

Figure 9:

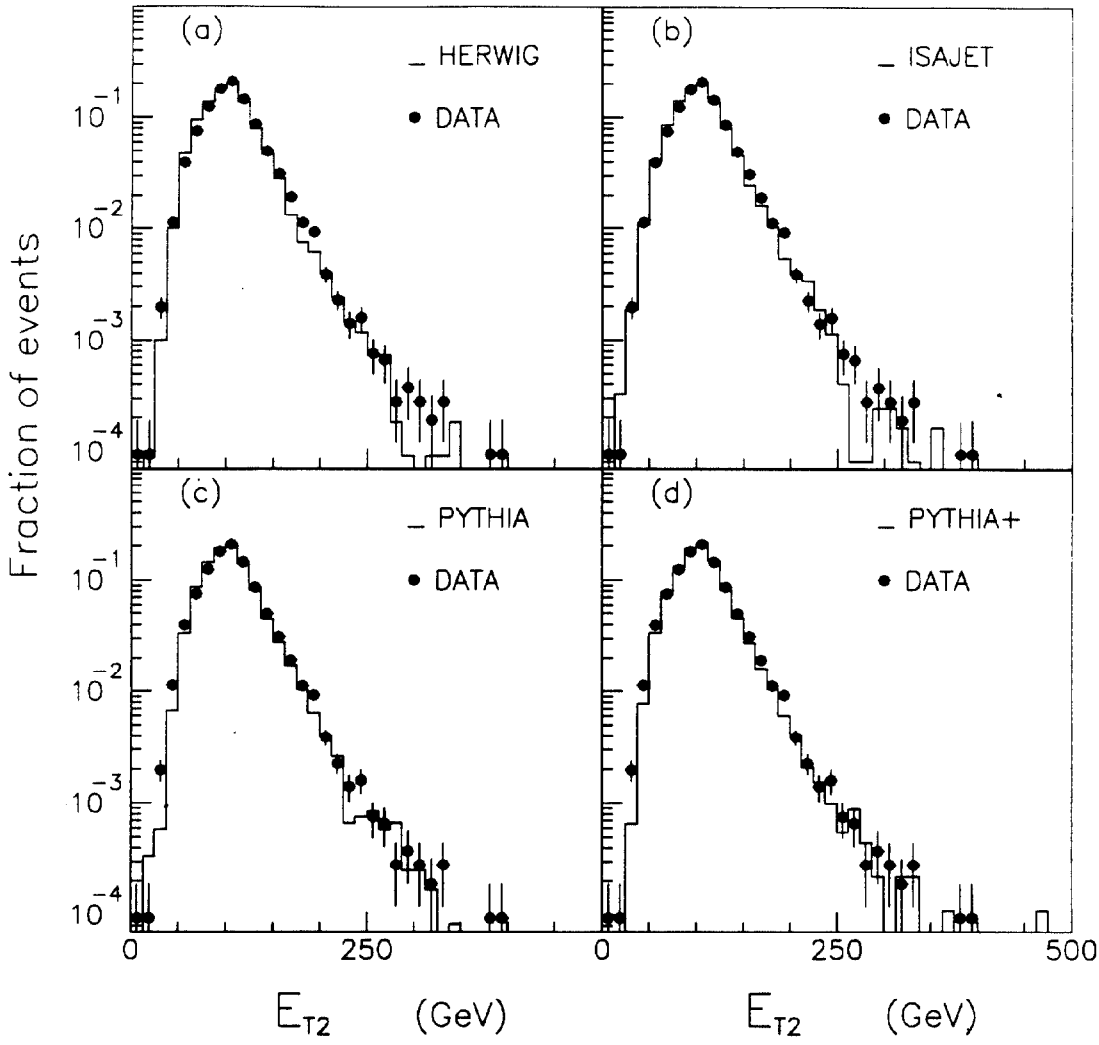
(a)
HERWIG
DATA
(b)
ISAJET
DATA
(c)
PYTHIA
DATA
(d)
PYTHIA+
DATA
Fraction of events
10^{-1}
10^{-2}
10^{-3}
10^{-4}
0
250
500
E_{T2} (GeV)

Figure 10:

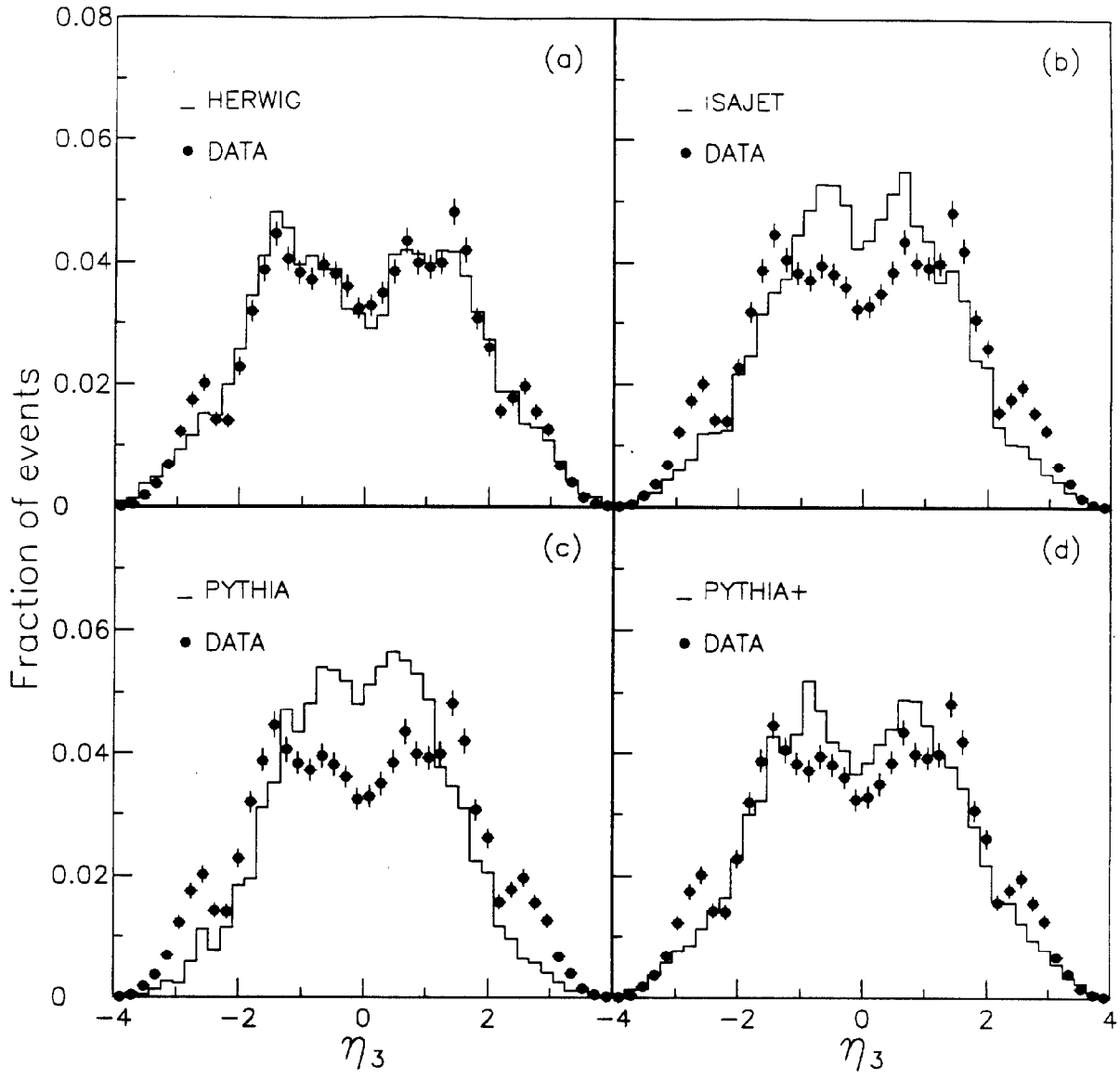
0.08
0.06
0.04
0.02
0
Fraction of events
(a)
HERWIG
DATA
(b)
ISAJET
DATA
(c)
PYTHIA
DATA
(d)
PYTHIA+
DATA
−4
−2
0
2
4
η_3

Figure 11:

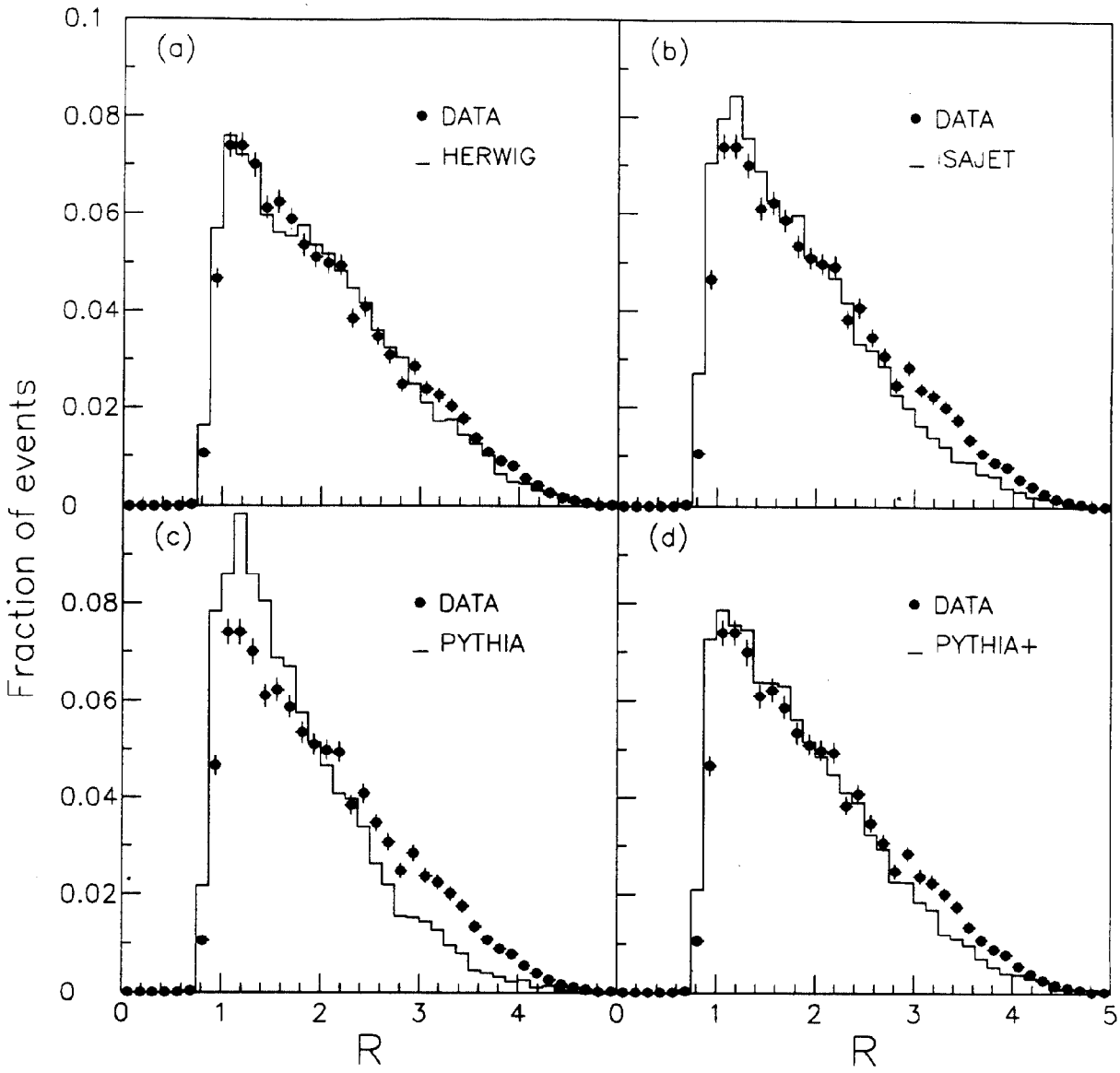
(a)
DATA
HERWIG
(b)
DATA
ISAJET
(c)
DATA
PYTHIA
(d)
DATA
PYTHIA+
Fraction of events
R
R
0.1
0.08
0.06
0.04
0.02
0
0
1
2
3
4
5

Figure 12:

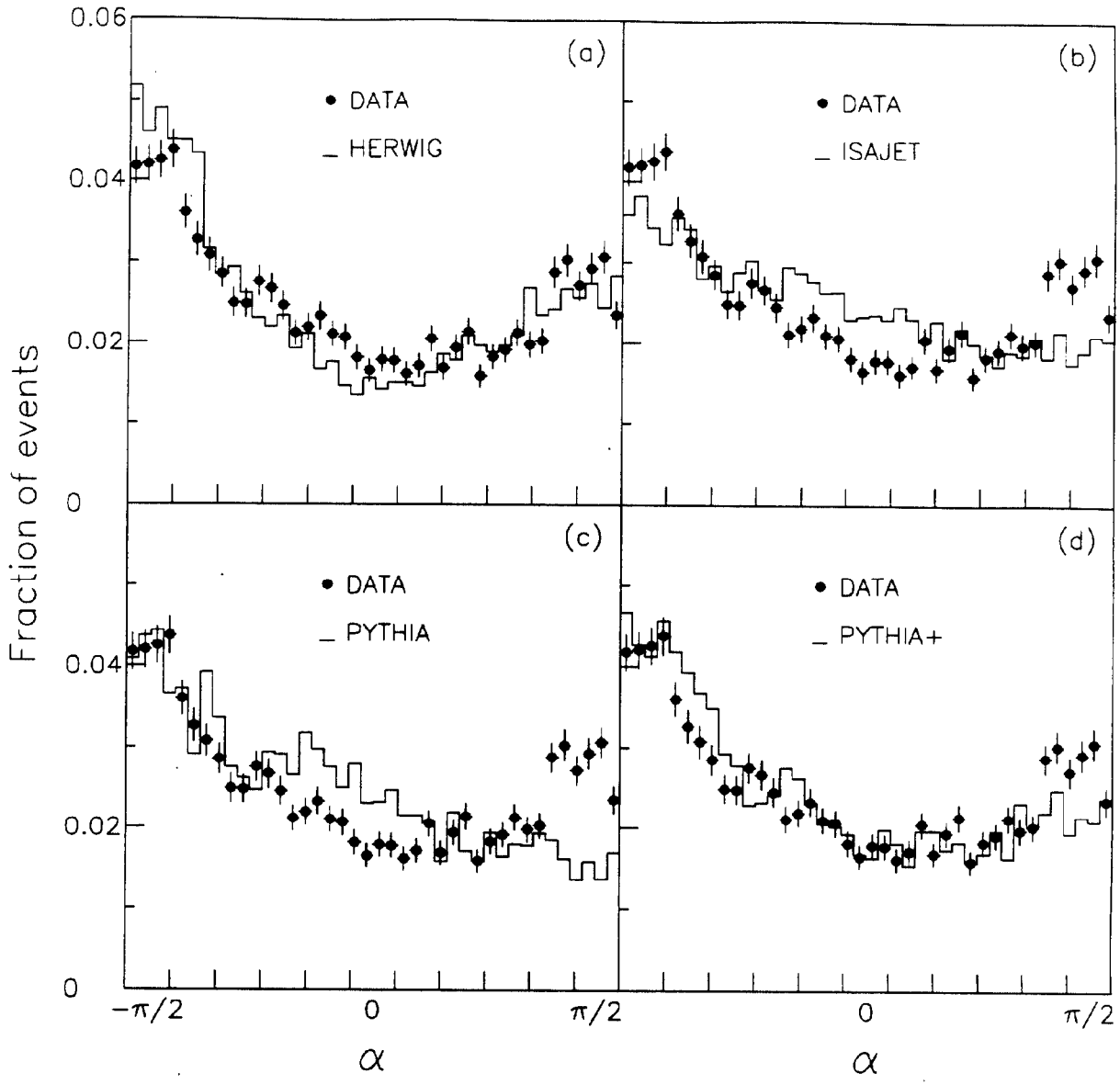
0.06
0.04
0.02
0
Fraction of events
(a)
• DATA
_ HERWIG
(b)
• DATA
_ ISAJET
(c)
• DATA
_ PYTHIA
(d)
• DATA
_ PYTHIA+
−π/2
0
π/2
α

Figure 13:

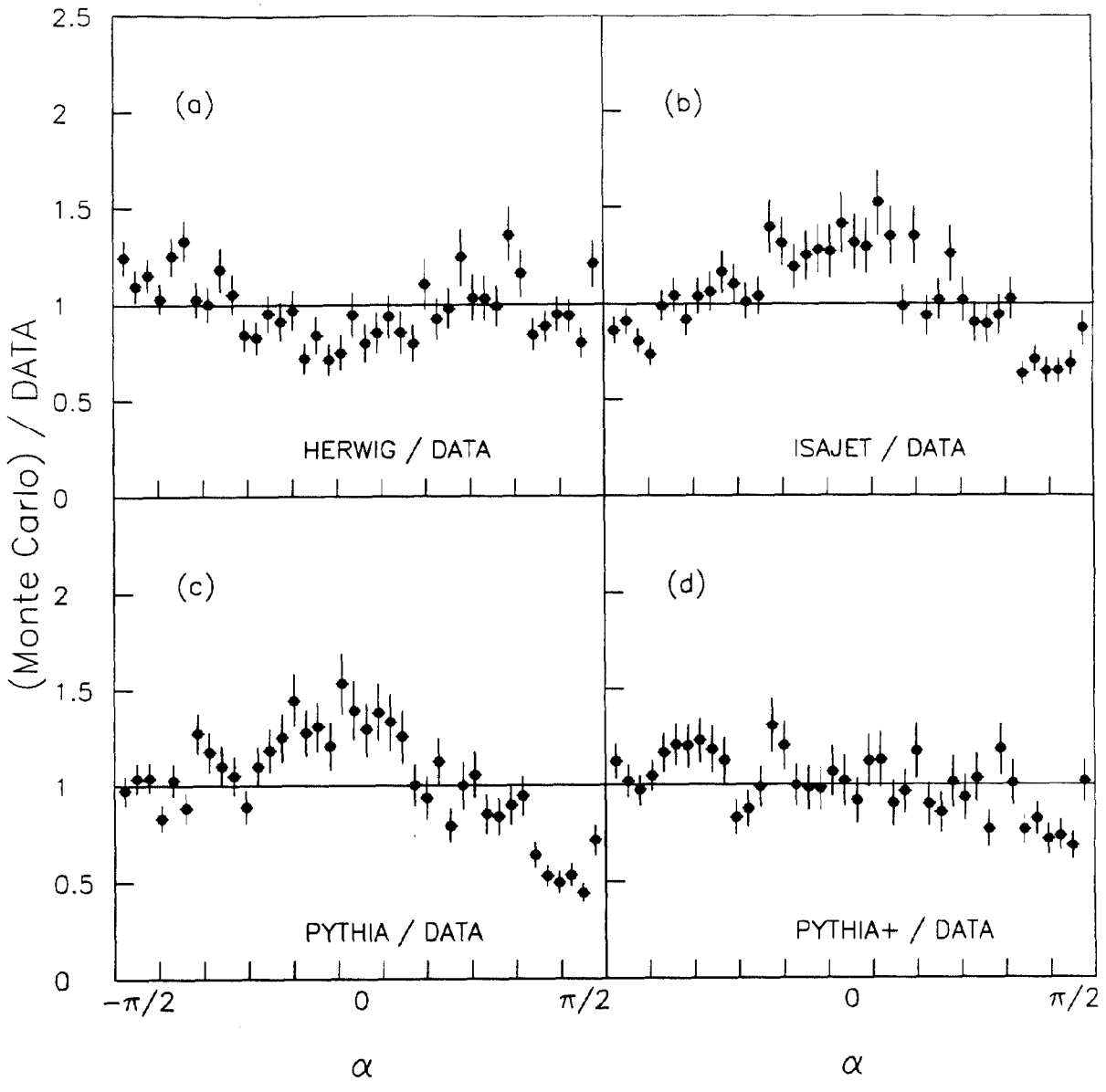
(a)
(b)
(c)
(d)
HERWIG / DATA
ISAJET / DATA
PYTHIA / DATA
PYTHIA+ / DATA
(Monte Carlo) / DATA
2.5
2
1.5
1
0.5
0
−π/2
0
π/2
α

Figure 14: